The Histone Demethylase FBXL10 Regulates the Proliferation of Spermatogonia and Ensures Long-Term Sustainable Spermatogenesis in Mice 1

Authors: Ozawa, Manabu, Fukuda, Tsuyoshi, Sakamoto, Reiko, Honda, Hiroaki, and Yoshida, Nobuaki

Source: Biology of Reproduction, 94(4)

Published By: Society for the Study of Reproduction

URL: https://doi.org/10.1095/biolreprod.115.135988

BIOLOGY OF REPRODUCTION (2016) **94**(4):92, 1–11
Published online before print 16 March 2016.
DOI 10.1095/biolreprod.115.135988

The Histone Demethylase FBXL10 Regulates the Proliferation of Spermatogonia and Ensures Long-Term Sustainable Spermatogenesis in Mice[1]

Manabu Ozawa,[2,4] Tsuyoshi Fukuda,[4] Reiko Sakamoto,[4] Hiroaki Honda,[5] and Nobuaki Yoshida[3,4]

[4]*Laboratory of Developmental Genetics, Center for Experimental Medicine and Systems Biology, The Institute of Medical Science, The University of Tokyo, Tokyo, Japan*
[5]*Department of Disease Model, Research Institute of Radiation Biology and Medicine, Hiroshima University, Hiroshima, Japan*

ABSTRACT

The F-box and leucine-rich repeat protein 10 (*Fbxl10*) gene encodes a protein that catalyzes demethylation of H3K4 and H3K36. In this study, we show the important roles of FBXL10 as a histone demethylase in sustainable sperm production using mice in which the JmjC domain of *Fbxl10* was deleted (*Fbxl10*$^{DeltaJ/DeltaJ}$). In histological analysis, testis sections from 10-wk-old *Fbxl10*$^{DeltaJ/DeltaJ}$ mice appeared normal. On the other hand, testes from 7-mo-old *Fbxl10*$^{DeltaJ/DeltaJ}$ mice contained a greater ratio of seminiferous tubules exhibiting degeneration of spermatogenesis. Further analysis using an in vitro spermatogonia culture system, that is, germline stem cells (GSCs), revealed that *Fbxl10*$^{DeltaJ/DeltaJ}$ GSCs expressed a significantly higher level of *P21* and *P19* mRNA, cyclin-dependent kinase inhibitors and also known as cellular senescence markers, than wild-type (WT) GSCs. Furthermore, the ratio of *Fbxl10*$^{DeltaJ/DeltaJ}$ GSCs in G0/G1 phase was higher and the ratios in S and G2/M phases were lower than the corresponding ratios of WT GSCs, and the doubling speed of *Fbxl10*$^{DeltaJ/DeltaJ}$ GSCs was significantly slower than that of WT GSCs. In addition to these in vitro results, an in vivo study indicated that recovery of spermatogenesis after a transient reduction in the number of testicular germ cells by busulfan treatment was significantly slower in *Fbxl10*$^{DeltaJ/DeltaJ}$ mice than in WT mice. These data suggest that *Fbxl10* plays important roles in long-term sustainable spermatogenesis via regulating cell cycle.

cell cycle, epigenetics, spermatogenesis, spermatogonia, spermatogonial stem cells

INTRODUCTION

In male mice, spermatogenesis starts as early as Postnatal Day 3 (PD3). After several rounds of mitotic cell proliferation, spermatogonia enter meiosis. Meiotic cells termed spermatocytes undergo two successive rounds of cell division and become haploid spermatids. After an additional maturation period termed spermiogenesis, mobile and fertile spermatozoa first appear at around PD35. Spermatogenesis is then sustained throughout life under the control of molecular mechanisms, including epigenetics, which orchestrate proper gene expression [1–3].

Epigenetic modifications such as DNA methylation and histone modifications control gene expression either positively or negatively, play essential roles in the proper development of specific tissues, and confer cellular identity. The methylation status of histone lysine residues, which is spatiotemporally balanced by the activities of histone methyltransferases and histone demethylases, is an important epigenetic modification. A number of studies using gene knockout mouse models revealed that proper histone modifications are crucial for germ cell development and sustainable spermatogenesis [1, 2, 4]. For example, a lack of *Jmjd1c,* which encodes a H3K9 demethylase, causes age-dependent infertility accompanied by a progressive reduction in the number of germ cells [5]. Proper maintenance of H3K4 methylation is crucial for fertility because knockout of the H3K4 methyltransferase-encoding gene *Kmt2b*/*Mll2* or *Prdm9*/*Meisetz* results in an infertile phenotype in both males and females [6, 7]. Similarly, a lack of *Kdm1b*/*Lsd2*, which encodes a histone lysine demethylase that catalyzes demethylation of H3K4, causes defects in proper genomic imprinting, resulting in infertility in female mice, whereas male gene knockout mice show no distinct abnormal phenotype and their reproductive performance is unaffected [8].

F-box and leucine-rich repeat protein 10 (FBXL10, also called KDM2B and JHDM1B) is a histone lysine demethylase possessing the histone lysine demethylase catalytic domain JmjC and catalyzes demethylation of H3K4 [9, 10] and/or H3K36 [11, 12]. In mice, *Fbxl10* is expressed in many tissues such as the thymus, brain, heart, and lung, but its expression intensity is more pronounced in the testis [13]. *Fbxl10* has two different isoforms, a longer full-length (FL) isoform contains the catalytic domain for histone demethylation JmjC and a short-form (SF) isoform that lacks the JmjC domain although other catalytic domains such as the F-box domain (protein-binding), CXXC-zinc finger domain (DNA-binding), PHD domain, and leucine-rich repeats are the same as in the FL isoform. Recently, we established a gene knockout mouse model in which JmjC domain-containing *Fbxl10-FL* was deleted (Fbxl10 ΔJmjC/ΔJmjC, *Fbxl10*$^{\Delta J/\Delta J}$) and demonstrated that a lack of *Fbxl10-FL* causes a significant increase in the occurrence of a neural tube defect during prenatal development resulting in prenatal death, although some *Fbxl10*$^{\Delta J/\Delta J}$ mice do not exhibit this lethal phenotype and reach adulthood [13]. Interestingly, *Fbxl10*$^{\Delta J/\Delta J}$ adult male mice have significantly fewer sperm in the epididymis [13]. Our results, together with those of reports showing the importance of proper histone

[1]Supported in part by Grants from the Ministry of Education, Culture, Sports and Technology (MEXT), Japan (to M.O.), and carried out at the Joint Usage/Research Center (RIRBM), Hiroshima University.
[2]Correspondence: E-mail: semil@ims.u-tokyo.ac.jp
[3]Correspondence: E-mail: nobuaki@ims.u-tokyo.ac.jp

Received: 2 October 2015.
First decision: 5 November 2015.
Accepted: 8 March 2016.

eISSN: 1529-7268 http://www.biolreprod.org
ISSN: 0006-3363

modifications for germ cell development and/or spermatogenesis, led us to hypothesize that *Fbxl10-FL* might be important for sustainable spermatogenesis. Therefore, in the present study, we aimed to investigate the roles of *Fbxl10-FL* in spermatogenesis. A gene knockout mouse model that we previously established revealed that although $Fbxl10^{\Delta J/\Delta J}$ males were fertile at least when they were 1 yr old, a lack of *Fbxl10* caused a progressive increase in the number of seminiferous tubules showing degeneration of spermatogenesis, accompanied by a drastic alteration in the distribution of H3K4me3 in testicular germ cells. Furthermore, cultured spermatogonia, that is, germline stem cells (GSCs), lacking *Fbxl10-FL* expressed a significantly higher level of the cellular senescence markers *P21* and *P19* and proliferated significantly slower than wild-type (WT) cells. Our present data indicate that FBXL10 ensures long-term sustainable spermatogenesis via regulating the cell cycle.

MATERIALS AND METHODS

Animals and Ethics Statement

Mice were housed under pathogen-free conditions in the experimental animal facility at the University of Tokyo. All mouse experiments were approved by the Institutional Animal Care and Use Committee of the University of Tokyo (approval number PA10-59) and performed in compliance with their guidelines. DBA/2JJcl mice were purchased from Clea-Japan, and C57B6/J mice were purchased from Japan SLC. $Fbxl10^{\Delta J/\Delta J}$ mice used in this study were produced in our laboratory as previously reported [13] and have a mixed genetic background (129, C57BL/6J, and DBA/2JJcl).

Isolation of Testicular Germ Cells for Development of GSCs

For development of GSCs, testes from mice at Postpartum Day 5–7 were harvested and digested into single cells as reported previously [14–16]. Single cells were washed twice with PBS containing 1 mM ethylenediaminetetraacetic acid (EDTA) and 1% (w/v) bovine serum albumin (BSA), and $THY1.2^{+}$ cells, the fraction in which spermatogonial stem cells are enriched [14, 15, 17], were sorted by magnetic-activated cell sorting. Collected cells were cultured to develop into stably self-renewing GSCs (Fig. 3A) on mitotically inactivated feeder cells, that is, x-ray-irradiated mouse embryonic fibroblasts (MEFs), in medium as previously reported [18] with slight modifications. Specifically, 2 mM GlutaMax or 5 mg/ml AlbuMax II (both from Life Technologies) were added to the medium instead of 2 mM L-glutamine and 5 mg/ml BSA, respectively. The medium was changed every 3–4 days. GSCs were passaged every 7–10 days using 0.25% (w/v) trypsin solution and seeded at a density of $1–2 \times 10^5$ cells/ml on feeder MEFs.

RNA Quantification in Testes or GSCs by Quantitative Real-Time PCR

Total RNA was extracted from testes using Sepasol-RNA I super G (Nacalai Tesque) according to the manufacturer's instructions and treated with DNaseI (Takara) to digest potentially contaminating genomic DNA. Total RNA was extracted from cultured GSCs using NucleoSpin RNA II (Macherey-Nagel) according to the manufacturer's instructions (DNase treatment was included in the RNA extraction procedure in this kit). Total RNA (500–800 ng) was used to synthesize cDNA using SuperScript VILO (Life Technologies) according to the manufacturer's instructions in a reaction volume of 10 μl, which was diluted 2-fold with water after the reverse transcription reaction. The synthesized cDNA was used for quantitative real-time PCR analysis (Applied Biosystems StepOne; Life Technologies) in a PCR reaction mixture of 10 μl containing 1× FastSYBR Green mix (Life Technologies) and 0.3 μM each of the forward and reverse primers. The fold difference was calculated using the $\Delta\Delta C_t$ method [19] with *Gapdh* as the reference. The primer sequences used in this study are shown in Table 1.

Histological Analysis

Testes were fixed in PBS containing 4% (w/v) paraformaldehyde overnight at 4°C and then dehydrated by serial treatment with gradient ethanol solutions (from 20% to 100% [v/v] ethanol). Thereafter, dehydrated testes were embedded in paraffin for sectioning. Sections were cut at a thickness of 5 μm. For histological staining, sections were deparaffinized in Lemosol A (Wako), rehydrated by serial treatment with gradient ethanol solutions (from 100% to 70% [v/v] ethanol), and stained with hematoxylin-eosin (HE). Paraffin-embedded sections were also used for immunohistochemistry as described below.

Immunohistochemistry

Paraffin-embedded sections were deparaffinized and rehydrated as described above. Rehydrated sections were boiled in sodium citrate buffer (10 mM sodium citrate and 0.05% [v/v] Tween-20 prepared in water, pH 6.0) or Tris-EDTA buffer (10 mM Tris, 1 mM EDTA, and 0.05% [v/v] Tween-20 prepared in water, pH 9.0) using autoclaving (105°C, 15 min) to reactivate antigens, blocked in PBS containing 0.1% (v/v) Triton-X and 5% (w/v) BSA for 1 h at room temperature, and exposed to primary antibodies overnight at 4°C. Immunoreactivity was visualized using Alexa Fluor 488-, 555-, or 647-conjugated host animal-specific secondary antibodies (Life Technologies) and observed using a microscope capable of detecting fluorescein (BZ-9000; Keyence). The primary antibodies used were as follows: rabbit anti-FBXL10 (1:200; 09-864; Merck Millipore), rabbit anti-H3K36me1 (1:100; ab9048; Abcam), rabbit anti-H3K36me2 (1:25; 2901; Cell Signaling Technology), rabbit anti-H3K36me3 (1:100; 4909; Cell Signaling Technology), rabbit anti-H3K4me3 (1:200; 9727; Cell Signaling Technology), rabbit anti-PLZF (1:50; sc-22839; Santa Cruz), goat anti-GATA4 (1:400; sc-1237; Santa Cruz), rabbit anti-WT1 (1:50; sc-192; Santa Cruz), rat anti-germ cell-specific nuclear antigen (GENA) (1:2000; clone TRA98; BioAcademia), goat ant-SCP3 (1:100; sc-20845; Santa Cruz), and rat anti-Ki67 (1:100; clone 16A8; BioLegend).

Western Blot Analysis

Protein was extracted from GSCs by sonication in RIPA buffer and analyzed by standard Western blot analysis protocols with the same set of methylation-specific anti-H3 primary antibodies as used in the immunohistochemistry. Rabbit anti-H3 antibody (1:5000; ab1791; Abcam) was also used to detect total H3. Secondary horseradish peroxidase-conjugated donkey anti-rabbit immunoglobulin G (GE healthcare Japan) was used to visualize each protein with Luminata Forte (Merck Millipore).

Flow Cytometry

For cytometric analysis to detect cell surface proteins, cells were incubated with PerCP/Cy5.5-conjugated anti-EpCAM (1:2500; clone G8.8; BioLegend), APC-conjugated anti-c-KIT (1:25000; clone 2B8; BioLegend), and Alexa Fluor 488-conjugated anti-ITGA6 (1:500; clone GoH3; BioLegend) antibodies at 4°C for 45 min in PBS containing 2 mM EDTA and 1% (w/v) BSA. To detect intracellular cleaved CASPASE-3, cells were fixed with 1% (v/v) paraformaldehyde prepared in PBS for 10 min at room temperature and then permeabilized using 90% (v/v) ice-cold methanol for 30 min. Permeabilized cells were incubated with a rabbit anti-cleaved CASPASE-3 antibody (1:400; 9664; Cell Signaling Technology) at 4°C for 45 min and then exposed to Alexa Fluor 647-conjugated anti-rabbit immunoglobulin G (Life Technologies) at 4°C for 45 min. For cell cycle analysis, cells were fixed and permeabilized in 90% (v/v) ethanol prepared in PBS overnight at −20°C. Thereafter, DNA was stained with 200 μg/ml propidium iodide (Sigma-Aldrich) and endogenous RNA was simultaneously digested with 50 μg/ml RNase A (Merck Millipore) for 20 min at 37°C. Stained cells were analyzed using the FACS Calibur system (BD Biosciences).

Busulfan Administration to Adult Male Mice

Male mice aged 8 wk old were intraperitoneally administered busulfan (B2635; Sigma-Aldrich) at a dose of 30 μg/g body weight. Testes were collected 2, 4, or 8 wk after administration and subjected to histological or flow cytometric analysis.

Statistical Analysis

All numerical data are shown as the mean ± SEM of three independent replications. Differences between genotypes were tested using the Student *t*-test. *P* values less than 0.05 were considered significant.

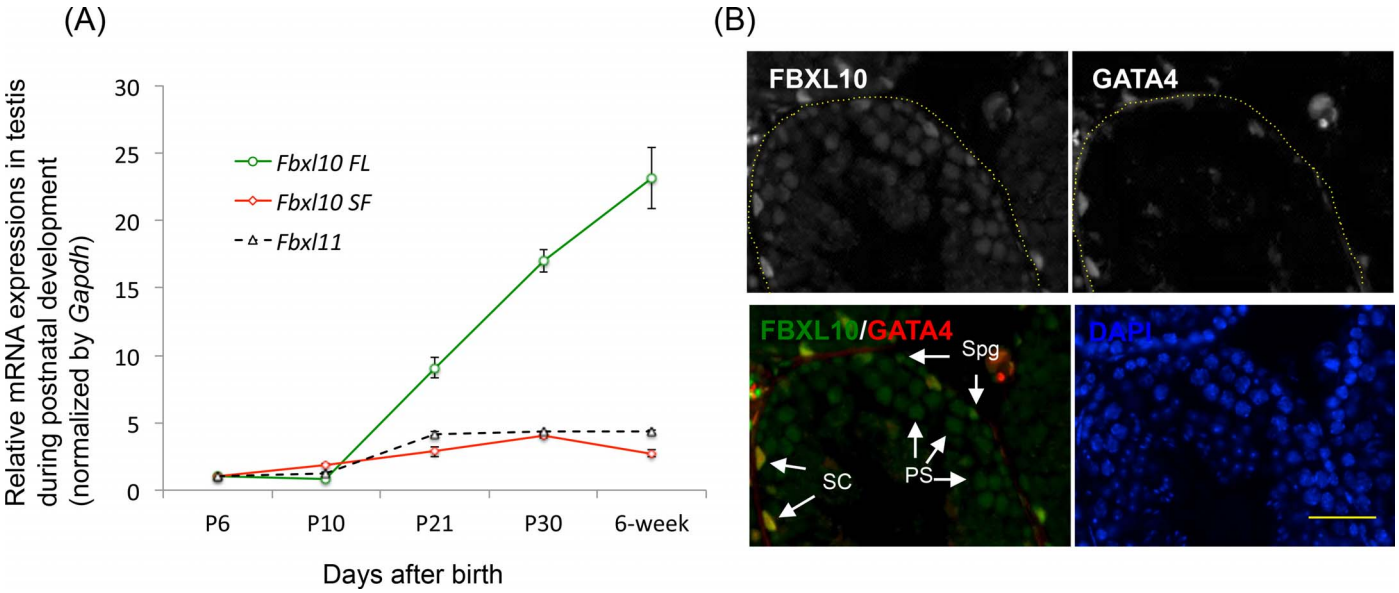

FIG. 1. Spatiotemporal expression of *Fbxl10* in murine testes. **A**) Quantitative real-time PCR analysis of *Fbxl10-FL, Fbxl10-SF,* and *Fbxl11* in testes during postnatal development. Gene expression was standardized using *Gapdh,* and the expression level of each gene at PD6 was designated as 1-fold (n = 3 per point). **B**) Immunohistochemical analysis of FBXL10 and GATA4 (Sertoli cells) in 9-wk-old testes. Nuclei were stained with 4′,6-diamidino-2-phenylindole. SC, Sertoli cell; Spg, spermatogonia; and PS, pachytene spermatocyte (bar = 50 μm).

RESULTS

Fbxl10 *Expression in Testes During Postnatal Development*

To investigate the fluctuation in *Fbxl10* expression in testes during postnatal development, both isoforms of *Fbxl10* mRNA (i.e., *Fbxl10-FL* and *Fbxl10-SF*) extracted from WT C57B6/J strain were measured using quantitative PCR. In addition, mRNA expression of a homologous gene of *Fbxl10,* termed *Fbxl11,* which shares the same set of functional domains including the histone demethylase JmjC domain [20], was also measured. Although *Fbxl10-FL* expression did not change much between PD6 and PD10, it was 9.07 ± 0.73 fold higher at PD21 than at PD6 and was further increased at 6 wk of age (23.17 ± 2.28 fold higher than at PD6) (Fig. 1A). On the other hand, although expression of *Fbxl10-SF* was also higher at PD30 than at PD6, this increase was less evident than that in *Fbxl10-FL*. The fluctuations in *Fbxl11* and *Fbxl10-SF* exhibited a similar pattern, that is, expression was slightly increased until PD21–PD30 and remained roughly constant thereafter until 6 wk of age (Fig. 1A). These different expression patterns suggest that *Fbxl10-FL* and *Fbxl10-SF* are differentially regulated in different types of testicular cells. Next, to determine the expression of FBXL10 protein in testes, immunohistochemistry was performed using testes from 9-wk-old WT male. FBXL10 labeling was detected in spermatogonia and spermatocytes as well as GATA4^{+} somatic Sertoli cells, whereas the signal was low or absent in haploid spermatids (Fig. 1B and Supplemental Fig. S1; Supplemental Data are available online at www.biolreprod.org).

Fbxl10$^{\Delta J/\Delta J}$ *Mice Exhibit an Altered H3K4me3 Pattern in Testicular Germ Cells and Spermatogenesis Deficiency in an Age-Dependent Manner*

Several studies reported that FBXL10 specifically catalyzes demethylation of H3K36me1/me2/me3 or H3K4me3 [9, 11, 21]. Thus, to determine the global methylation patterns of H3K36 and H3K4 in *Fbxl10*$^{\Delta J/\Delta J}$ testes, immunohistochemistry using specific antibodies was performed. No significant differences in the distribution of H3K36me1/me2 or me3 between WT and *Fbxl10*$^{\Delta J/\Delta J}$ testes was detected (Fig. 2A). On the other hand, the distribution pattern of H3K4me3 differed between *Fbxl10*$^{\Delta J/\Delta J}$ testes and age-matched WT testes. In WT testes, the H3K4me3 signal was most evident in SCP3^{+} primary spermatocyte (seminiferous stage I–III) or spermatogonia (seminiferous stage IX–XI), and the signal was weaker in cells that went beyond the first meiosis. By contrast, although the H3K4me3 signal was detected in SCP3^{+} primary spermatocyte or spermatogonia in *Fbxl10*$^{\Delta J/\Delta J}$ testes, it was stronger in postmeiotic spermatids (Fig. 2B). We previously reported that the number of sperm is significantly lower (~2-fold) in *Fbxl10*$^{\Delta J/\Delta J}$ mice than in age-matched controls [13]. Thus, in the present study, we determined the importance of *Fbxl10-FL* in spermatogenesis. Testes from *Fbxl10*$^{\Delta J/\Delta J}$ mice were histologically analyzed. No significant difference in HE-stained testis sections was observed between 10-wk-old WT and *Fbxl10*$^{\Delta J/\Delta J}$ mice, whereas the number of seminiferous tubules exhibiting degeneration of spermatogenesis was significantly higher in testes of 7-mo-old *Fbxl10*$^{\Delta J/\Delta J}$ mice than in those of age-matched WT mice (n = 3 different mice for each age and genotype, and 108–247 tubules were counted; Fig. 2, C and D). We also stained for the Sertoli cell marker WT1. WT1^{+} Sertoli cells were present even in abnormal seminiferous tubules that lacked germ cells (Supplemental Fig. S2). These results suggest that FBXL10 is not essential for spermatogenesis, at least during younger age, but regulates the H3K4me3 status in testicular germ cells and plays a role(s) in sustaining spermatogenesis for a long period.

Fbxl10$^{\Delta J/\Delta J}$ *GSCs Exhibit Slower Growth In Vitro and Increased Expression of the Cyclin-Dependent Kinase Inhibitor (CDKI) P21 and P19*

FBXL10 reportedly regulates cell proliferation through CDKIs. Enhanced expression of *Fbxl10* activates the proliferation of human cancer cells [22, 23], whereas downregulation of *Fbxl10* induces an increase of P16 expression in embryonic fibroblasts of mice [24]. These studies and our present

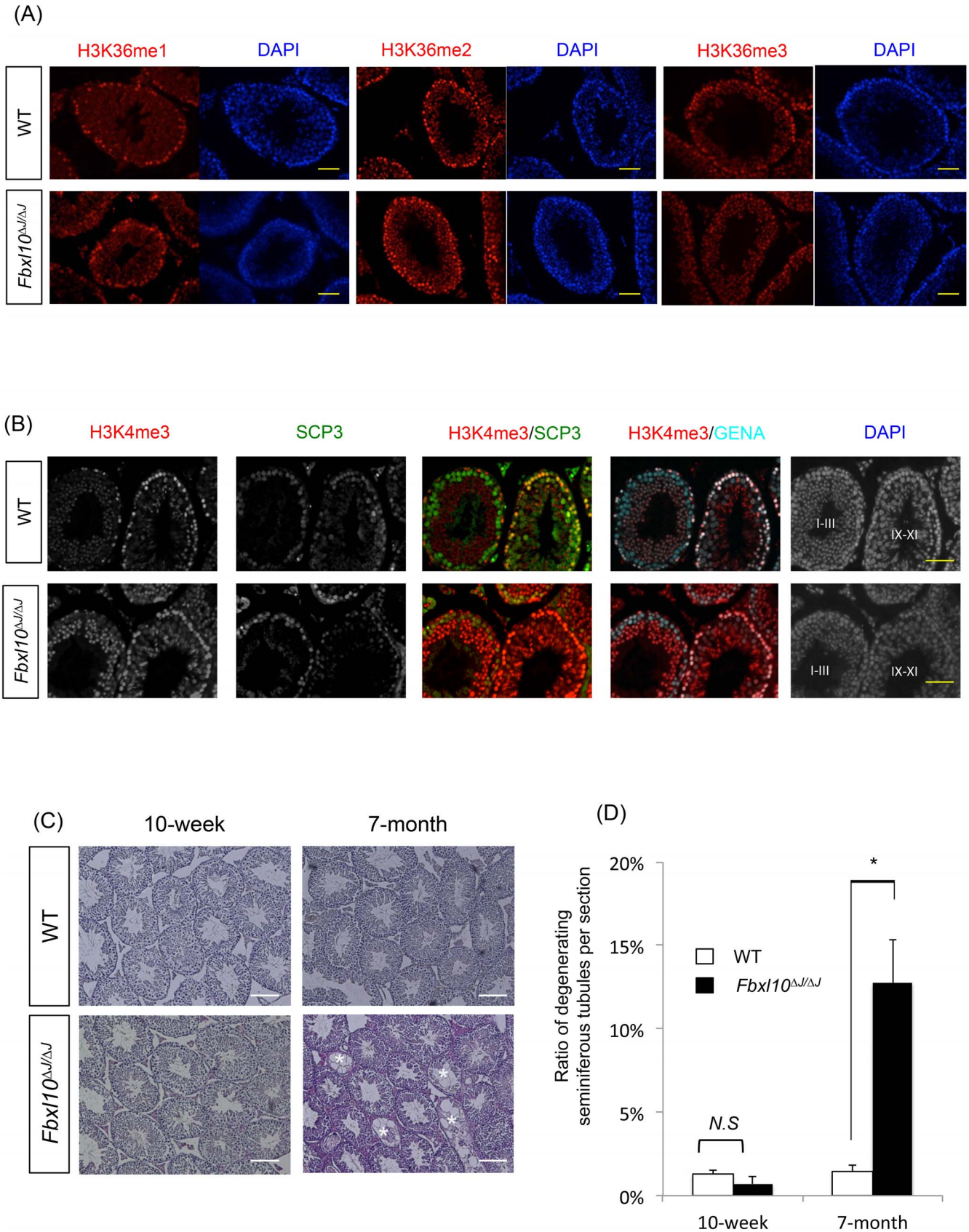

FIG. 2. Histological analysis of testes from *Fbxl10*$^{\Delta J/\Delta J}$ mice. **A** and **B**) Distribution of H3K36 and H3K4 methylation patterns in testes. Testes from *Fbxl10*$^{\Delta J/\Delta J}$ mice and age-matched WT mice were stained with an anti-H3K36me1/me2/me3 antibody (**A**) or an anti-H3K4me3 antibody (**B**) as well as for a first meiosis marker (SCP3) or a germ cell marker (GENA). 4′,6-Diamidino-2-phenylindole staining for nuclei is shown in the right panel (bar = 50 μm). **C**) HE staining of testes from 10-wk-old and 7-mo-old *Fbxl10*$^{\Delta J/\Delta J}$ mice and age-matched WT mice. Asterisks indicate seminiferous tubules exhibiting degeneration of spermatogenesis (bar = 100 μm). **D**) The graph shows the ratios of degenerating seminiferous tubules in *Fbxl10*$^{\Delta J/\Delta J}$ and WT mice. The asterisk depicts a significant difference (n = 3, $P < 0.05$).

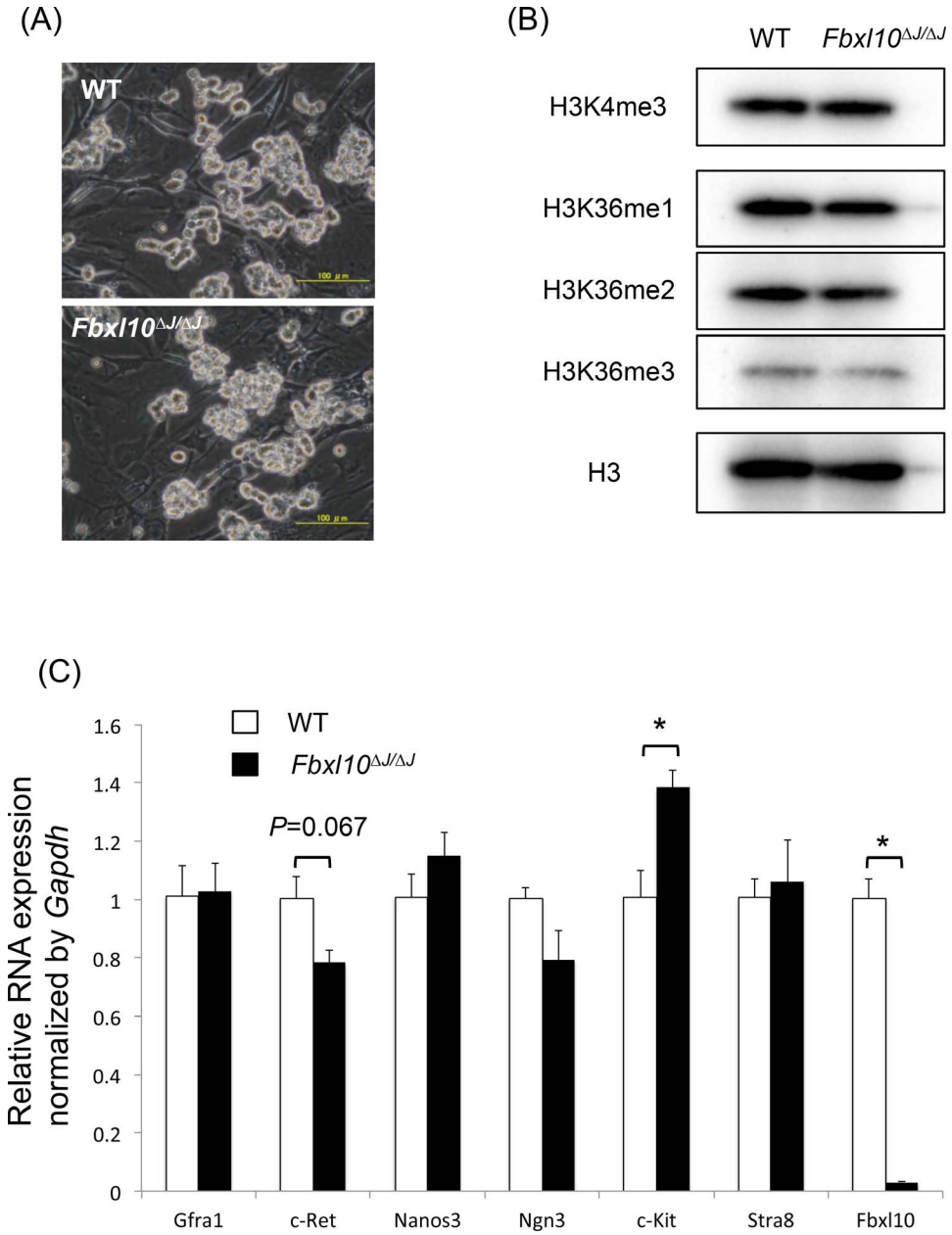

FIG. 3. In vitro characteristics of GSCs isolated from *Fbxl10*$^{\Delta J/\Delta J}$ mice. **A**) Representative morphology of GSCs isolated from WT (top) and *Fbxl10*$^{\Delta J/\Delta J}$ (bottom) mice. GSCs of both genotypes form grapelike colonies and self-renew on mitotically inactivated MEFs under stimulation with GDNF and FGF2. Bar = 100 μm. **B**) Western blot showing H3K4me3, and H3K36me1, 2, and 3 in GSCs. Pan-H3 was also analyzed as a loading control. Total protein was extracted from cells in their basic culture condition (GDNF and FGF2 on MEF). **C**) Quantitative real-time PCR analysis of spermatogonial marker genes. *Fbxl10* mRNA was also measured to ensure that the *Fbxl10* transcript was not expressed in *Fbxl10*$^{\Delta J/\Delta J}$ GSCs. Gene expression was standardized using *Gapdh,* and the expression level of each gene in WT GSCs was designated as 1-fold. The asterisk depicts a significant difference (n = 3, $P < 0.05$).

histological analysis that showed a progressive increase in the degeneration of spermatogenesis led us to hypothesize that cell cycle and/or proliferation of spermatogonia of *Fbxl10*$^{\Delta J/\Delta J}$ mice might be compromised. Undifferentiated spermatogonia can self-renew in vitro under stimulation with FGF2 and GDNF on feeder MEFs and possess stem/progenitor characteristics (GSCs) [14, 15, 25]. We took advantage of this culture system to evaluate the role of *Fbxl10-FL* in spermatogonia in vitro. GSCs have morphological features that are distinct from those of well-known pluripotent stem cells, such as embryonic stem cells (tightly aggregated and three-dimensional) and epiblast stem cells (flat and two-dimensional), and have a grapelike morphology [25]. GSCs lacking *Fbxl10-FL* also formed typical grapelike colonies, their shape was indistinguishable from that of WT GSCs (Fig. 3A), and they could proliferate for more than 25 passages. Using this GSC, we analyzed intensities of H3K4me3 as well as H3K36me1, 2, and 3 by Western blot analysis. There were no distinct differences in H3 methylations between *Fbxl10*$^{\Delta J/\Delta J}$ GSCs and WT GSCs (Fig. 3B). Next, we investigated the mRNA expression of six known spermatogonial marker genes by quantitative PCR. *Fbxl10-FL* mRNA was also measured to confirm knockout of *Fbxl10-FL* in our model. Little amplification of this gene was observed in *Fbxl10*$^{\Delta J/\Delta J}$ GSCs, confirming that these cells did not express *Fbxl10-FL* (Fig. 3C). Expression of *c-Ret,* a marker of undifferentiated spermatogonia, tended to be lower ($P =$

TABLE 1. Primer sequences used for quantitative real-time PCR.

Gene[a]	Forward	Reverse
Fbxl10 FL	GTTTCACTGACTTCCACATTGACTTT	GCAGGGTTGGAGGGATCAG
Fbxl10 SF	CCGAGGACGACGACTATGAATC	ACCTCCAAACTTCTTCATGTCCTT
Fbxl11	CTGTCTAATGAGTGTTCGAGGCTGC	GCCAATTCTCGTACAGCTCCAGG
Gfra1	CACTCCTGGATTTGCTGATGT	AGTGTGCGGTACTTGGTGC
c-Ret	ATTTCTCAAGGGATGCTTACTGG	GGTAGACGCCATAGAGATGCT
Nanos3	CACTACGGCCTAGGAGCTTGG	TGATCGCTGACAAGACTGTGGC
Ngn3	CCAAGAGCGAGTTGGCACT	CGGGCCATAGAAGCTGTGG
c-Kit	GCCACGTCTCAGCCATCTG	GTCGCCAGCTTCAACTATTAACT
Stra8	CCTGGTTGAGGGGTGTAAGG	ATCACAGCCCTGTCACTGC
P21	GAACATCTCAGGGCCGAAAA	GCGCTTGGAGTGATAGAAATCTG
P19	GCTCTGGCTTTCGTGAACATG	TCGAATCTGCACCGTAGTTGAG
P16	CCCAACGCCCCGAACT	AACGTTGCCCATCATCATCA
P15	AGATCCCAACGCCCTGAAC	CCCATCATCATGACCTGGATT
Gapdh	ATGAATACGGCTACAGCAACAGG	CTCTTGCTCAGTGTCCTTGCTG

[a] FL, full length; SF, short form.

0.067), whereas expression of *c-Kit,* a differentiated spermatogonia marker, was significantly higher in $Fbxl10^{\Delta J/\Delta J}$ GSCs than in WT GSCs, suggesting that $Fbxl10^{\Delta J/\Delta J}$ GSCs are predisposed to undergo differentiation to some extent (Fig. 3C).

Previous studies indicated that FBXL10 negatively regulates expression of CDKIs, of which hyperactivation causes retardation of cell proliferation [11, 26, 27]. Thus, we quantified mRNA expression of *P21, P19, P16,* and *P15*. The average expression levels of *P21, P19, P16,* and *P15* were higher in $Fbxl10^{\Delta J/\Delta J}$ GSCs than in WT GSCs, and the difference was significant in the cases of *P21* and *P19* (1.6-fold and 2.4-fold higher in $Fbxl10^{\Delta J/\Delta J}$ GSCs than in WT GSCs, respectively; Fig. 4A). CDKIs negatively regulate cell proliferation, and their enhanced expression causes the slower growth of many cell types [28]. Thus, we hypothesized that GSCs lacking *Fbxl10-FL* might exhibit altered proliferation. As anticipated, the doubling speed of $Fbxl10^{\Delta J/\Delta J}$ GSCs was significantly slower than that of WT GSCs (Fig. 4B). We also checked the frequency of apoptotic cells by immunostaining with an antibody against cleaved CASPASE-3, an indicator of apoptosis, and then performing flow cytometry. The frequency of apoptotic cells did not significantly differ between $Fbxl10^{\Delta J/\Delta J}$ and WT GSCs (Fig. 4C). Furthermore, cell cycle analysis using flow cytometry showed that the ratios of cells in G1/G0 phase and G2/M phase were higher and lower, respectively, among $Fbxl10^{\Delta J/\Delta J}$ GSCs than among WT GSCs, and these differences were significant (Fig. 4D). These results suggest that *Fbxl10-FL* regulates GSC proliferation by controlling progression of the cell cycle through CDKIs.

Loss of Fbxl10-FL *Reduces the Proliferation of Undifferentiated Spermatogonia In Vivo after Busulfan Treatment*

The results from the present in vitro study using $Fbxl10^{\Delta J/\Delta J}$ GSCs led us to hypothesize that the proliferative activity of spermatogonia might be suppressed in $Fbxl10^{\Delta J/\Delta J}$ mice. Therefore, we next determined mitotic activities of undifferentiated spermatogonia by immunohistochemistry with antibodies against PLZF, an undifferentiated spermatogonia marker, and Ki67, a mitotically active cell marker (Fig. 5A). The average number of $PLZF^+$ undifferentiated spermatogonia per tubule did not differ between $Fbxl10^{\Delta J/\Delta J}$ and age-matched WT (n = 3 different mice for each genotype, and 29–70 tubules were counted, Fig. 5B). In contrast, almost a half of $PLZF^+$ undifferentiated spermatogonia in WT testis were also $Ki67^+$, whereas mitotically inactive spermatogonia ($PLZF^+/Ki67^-$) were more evident in $Fbxl10^{\Delta J/\Delta J}$ testes (Fig. 5A, arrows), and the ratio was significantly higher in $Fbxl10^{\Delta J/\Delta J}$ than WT (n = 3 different mice for each genotype, and 303–685 PLZF-positive spermatogonia were counted; Fig. 5C). A transient reduction in the number of undifferentiated spermatogonia by administration of the cytotoxic alkylating agent busulfan reportedly causes an increase in mitotic division of undifferentiated spermatogonia [29, 30]. We also used this experimental model to determine the proliferation speed of undifferentiated spermatogonia in vivo by observing cellular recovery. The number of undifferentiated spermatogonia ($EpCAM^+/ITGA6^+/c\text{-}KIT^-$) [29, 31] at 2 wk after busulfan treatment did not differ between $Fbxl10^{\Delta J/\Delta J}$ and WT mice, whereas the number of these cells at 4 wk after administration was lower ($P = 0.08$) in $Fbxl10^{\Delta J/\Delta J}$ mice than in WT mice (Fig. 6A). Consistently, histological analysis showed that at 8 wk after injection, significantly fewer seminiferous tubules showed reconstitution of spermatogenesis in $Fbxl10^{\Delta J/\Delta J}$ mice than in WT mice (Fig. 6B). To assess the mitotic activity of undifferentiated spermatogonia, we stained busulfan-treated testes collected at 4 wk after injection with antibodies against PLZF and Ki67. The majority of $PLZF^+$ undifferentiated spermatogonia in WT testes were also $Ki67^+$. By contrast, spermatogonia that were $PLZF^+$ but $Ki67^-$ were more evident in $Fbxl10^{\Delta J/\Delta J}$ testes (Fig. 6C), and there were significantly more of these cells in $Fbxl10^{\Delta J/\Delta J}$ testes than in WT testes (n = 3 different mice for each genotype, and 193–474 PLZF-positive spermatogonia were counted, Fig. 6D). Together, the results from our $Fbxl10^{\Delta J/\Delta J}$ mouse model indicate that FBLX10 ensures long-term sustainable spermatogenesis by regulating cell proliferation.

DISCUSSION

In this study, we investigated the roles of *Fbxl10-FL* in spermatogenesis using a gene knockout mouse model. Our results demonstrated that a lack of *Fbxl10-FL* drastically altered the H3K4me3 distribution in testicular germ cells and there was an age-dependent increase in the number of seminiferous tubules exhibiting degeneration of spermatogenesis. An in vitro GSC culture model showed that $Fbxl10^{\Delta J/\Delta J}$ GSCs expressed a significantly higher level of *P21* and *P19,* cell cycle inhibitors and known as cellular senescence markers, and proliferated slower than WT GSCs. Furthermore, mitotically inactive undifferentiated spermatogonia was more evident in $Fbxl10^{\Delta J/\Delta J}$ mice than in WT mice and recovery of spermatogenesis in vivo after busulfan treatment was also significantly slower in $Fbxl10^{\Delta J/\Delta J}$ mice than in WT mice.

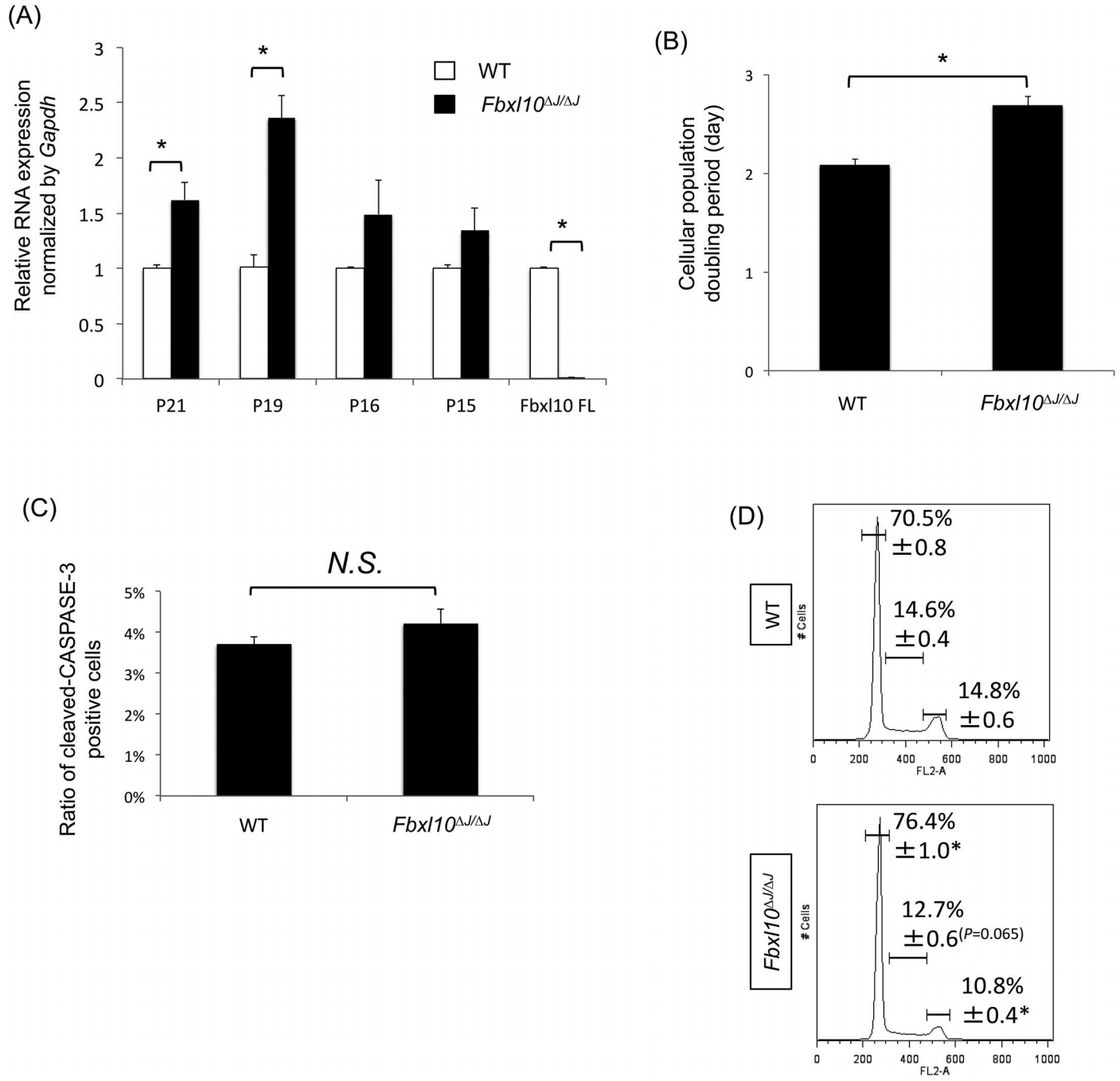

FIG. 4. Cell proliferation of GSCs isolated from *Fbxl10*$^{\Delta J/\Delta J}$ mice in vitro. **A**) Quantitative real-time PCR analysis of CDKI genes in *Fbxl10*$^{\Delta J/\Delta J}$ GSCs. Gene expression was standardized using *Gapdh,* and the expression level of each gene in WT GSCs was designated as 1-fold. The asterisk depicts a significant difference (n = 3, $P < 0.05$). **B**) Graph showing the doubling speeds of *Fbxl10*$^{\Delta J/\Delta J}$ and WT GSCs. The number of cells was counted in duplicate five times, and the doubling speed was calculated. The asterisk depicts a significant difference ($P < 0.05$). **C**) Ratio of apoptotic cells among *Fbxl10*$^{\Delta J/\Delta J}$ and WT GSCs as determined by immunostaining followed by flow cytometry. N.S., not significant. **D**) Cell cycle status of *Fbxl10*$^{\Delta J/\Delta J}$ and WT GSCs, and the percentages of cells in G0/G1, S, and G2/M phases (n = 3). The gates covering the left peak, the right peak, and the region in between these two peaks represent G0/G1, G2/M, and S phases, respectively. The asterisk depicts a significant difference ($P < 0.05$).

Taken together, our present data suggest that FBXL10 in spermatogonia plays important roles in long-term sustainable spermatogenesis.

Some recent papers reported that FBXL10 loss-of-function causes much severe phenotype than our *Fbxl10*$^{\Delta J/\Delta J}$, for example, *Fbxl10* mutant mice [32, 33] are totally embryonic lethal before 9–10 day postcoitum. In either previous case, loss of CxxC domain, through which FBXL10 binds to specific loci of the genome and regulates epigenetics of either DNA or histone as a component of Polycomb repressive complexes, is thought to be responsible for the lethality. In our mutant mouse, however, only the histone demethylase JmjC domain was deleted, and another *Fbxl10* isoform, that is, b *Fbxl10-SF,* which harbors CxxC, still remains functional. This may be a reason for explaining the difference of phenotypic intensity between our present results and the previous studies.

The proper regulation of H3K4 is important for fertility. For example, gene knockout of the H3K4 methyltransferase

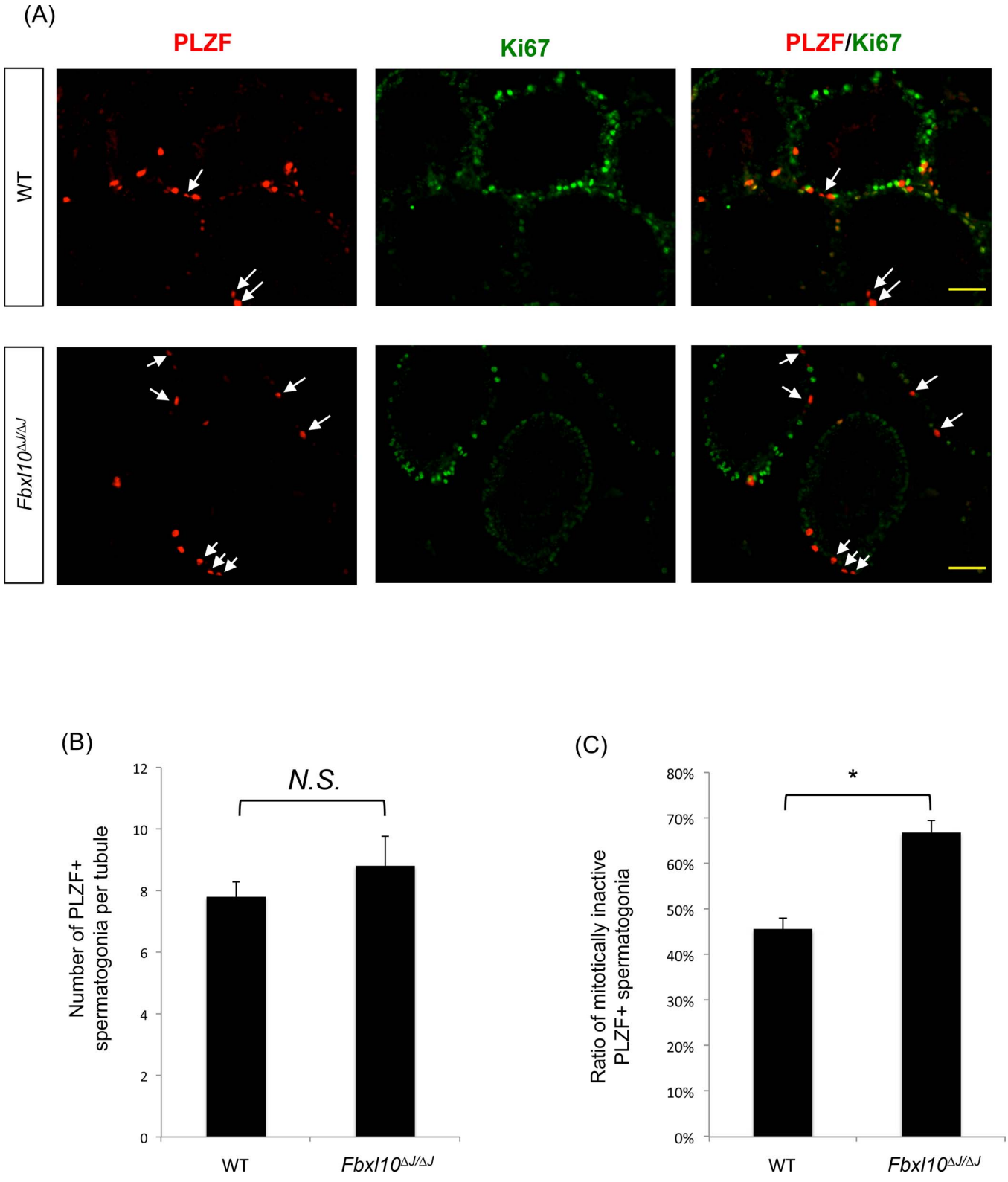

FIG. 5. Mitotic activity of undifferentiated spermatogonia in *Fbxl10*$^{\Delta J/\Delta J}$ mice. **A**) Immunohistochemistry of WT (top) and *Fbxl10*$^{\Delta J/\Delta J}$ (bottom) testes at 9 wk old. Sections were stained with anti-PLZF (marker of undifferentiated spermatogonia) and anti-Ki67 (marker of mitosis) antibodies. Arrows indicate mitotically inactive undifferentiated spermatogonia (PLZF^{+} and Ki67^{-}) (bar = 50 μm). **B**) The graph shows the number of undifferentiated spermatogonia per tubule. N.S., not significant. **C**) The graph shows the ratio of mitotically inactive undifferentiated spermatogonia. The asterisk depicts a significant difference (n = 3, $P < 0.05$).

Meisetz, which binds DNA at recombination hotspots and directs recombination during meiosis [34, 35], causes male infertility in mice, accompanied by a reduction in the H3K4me3 mark in testicular germ cells [6]. Our findings support the contribution of FBXL10-FL to the global H3K4me3 mark distribution in the testis (Fig. 2B). On the

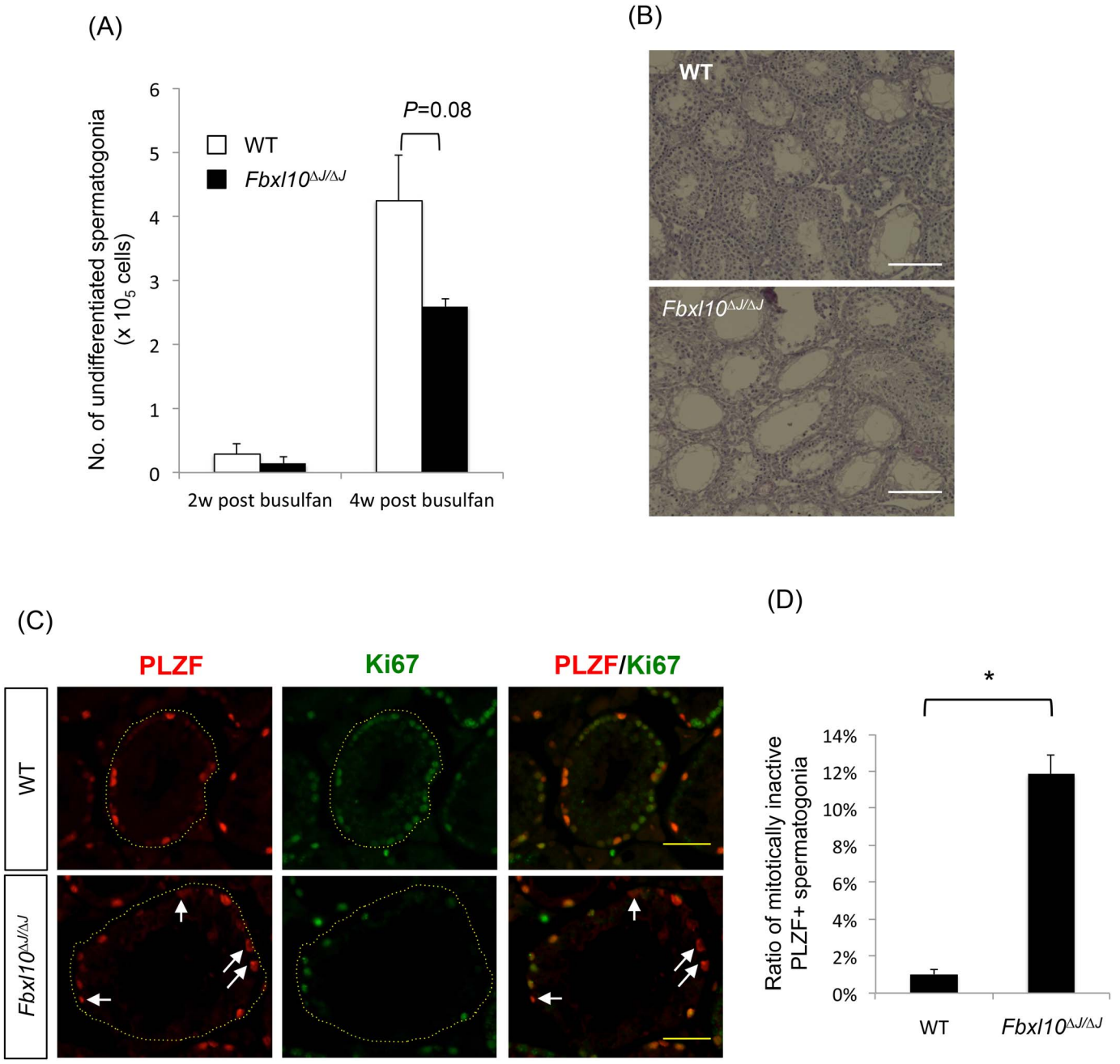

FIG. 6. Spermatogonial cell recovery after busulfan treatment is retarded in *Fbxl10*$^{\Delta J/\Delta J}$ mice. **A**) The numbers of undifferentiated spermatogonia (EpCAM$^+$/ITGA6$^+$/c-KIT$^-$) in *Fbxl10*$^{\Delta J/\Delta J}$ and WT testes after busulfan treatment as determined by flow cytometry (n = 3). **B**) Histological sections of WT (top) and *Fbxl10*$^{\Delta J/\Delta J}$ (bottom) testes at 8 wk after busulfan treatment (bar = 100 μm). **C**) Immunohistochemistry of WT (top) and *Fbxl10*$^{\Delta J/\Delta J}$ (bottom) testes at 4 wk after busulfan treatment. Sections were stained with anti-PLZF (marker of undifferentiated spermatogonia) and anti-Ki67 (marker of mitosis) antibodies. Arrows indicate mitotically inactive undifferentiated spermatogonia (PLZF$^+$ and Ki67$^-$) (bar = 50 μm). **D**) The graph shows the ratio of mitotically inactive undifferentiated spermatogonia. The asterisk depicts a significant difference (n = 3, $P < 0.05$).

other hand, spermatogenesis, at least at a young age, was not compromised by a lack of *Fbxl10-FL*. Therefore, *Fbxl10-FL* might be dispensable for spermatogenesis at this stage, despite the alteration in H3K4me3. Although FBXL10-FL and Meisetz share the same target histone residue, FBXL10-FL has demethylase activity, which is the opposite of Meisetz. Given that methylation of H3K4 is closely associated with transcriptional activation [36, 37], Meisetz is thought to function as a transcriptional activator whereas FBXL10 is thought to act as a transcriptional inhibitor. These differing roles might explain why our *Fbxl10*$^{\Delta J/\Delta J}$ male mice showed a different spermatogenesis phenotype than the previous generated knockout model. It is also possible that region-specific histone modifications of the genome are important for spermatogenesis. A mouse model lacking the histone H3K9-specific JmjC domain-containing protein JMJD1C exhibits an age-dependent abnormality in spermatogenesis, as in the present study, whereas no significant alteration in global histone modifications was detected by immunohistochemistry [5]. By contrast, Iwamori et al. [38] reported that knockout of a gene encoding another H3K9 demethylase, *Kdm4a*, clearly enhances the H3K9me3 mark in testicular germ cells, whereas no distinct

abnormal phenotype was observed in spermatogenesis. A further study is required to investigate the loci-specific histone methylation status in *Fbxl10*$^{\Delta J/\Delta J}$ testicular germ cells.

GSCs can self-renew in vitro and possess similar characteristics to in vivo undifferentiated spermatogonia, including stemness, under stimulation with GDNF and FGF2 [15, 25]. Interestingly, although *Fbxl10*$^{\Delta J/\Delta J}$ GSCs grew slower than WT GSCs, they could proliferate for at least 25 passages, equivalent to about 6–8 mo in spite of their age-dependent spermatogenesis degeneration phenotype in vivo. Similar results reported that a lack of *Plzf* increases the age-dependent degeneration of spermatogenesis, similar to the observation in our *Fbxl10*$^{\Delta J/\Delta J}$ mice [39, 40], whereas *Plzf*-null GSCs can be developed and maintained for a long time, although they grow slower than WT GSCs [41].

Using this in vitro model, we revealed that expression of *c-Ret* tended to be weaker ($P = 0.067$) and expression of c-Kit was significantly stronger in *Fbxl10*$^{\Delta J/\Delta J}$ GSCs than in WT GSCs (Fig. 3B). In testicular germ cells, c-RET expression is restricted to early undifferentiated spermatogonia, where c-RET dimerizes with GFRa1 and functions as a receptor for GDNF, an essential factor for spermatogonial stem cell self-renewal [42, 43]. By contrast, c-KIT is not expressed in undifferentiated spermatogonia, and its expression becomes evident in differentiating spermatogonia under stimulation with retinoic acid, a differentiation-initiating signal [44–46]. Therefore, *Fbxl10*$^{\Delta J/\Delta J}$ GSCs might tend to undergo differentiation to some extent. Interestingly, artificially aged GSCs, in which aging is induced by serial transplantation into testes followed by magnetic-activated cell sorting isolation using an anti-THY1.2 antibody also express a higher level of *c-Kit* [47], similar to *Fbxl10*$^{\Delta J/\Delta J}$ GSCs.

Aging or cellular senescence is a stress response that accompanies stable exit from the cell cycle [28]. A number of studies showed that *Fbxl10* has antisenescence roles in many types of cells through suppression of CDKI expression. For example, overexpression of *Fbxl10* can immortalize MEFs, and this effect is associated with suppression of the senescence-associated upregulation of either P16 or P15 [38, 47]. Similarly, forced expression of *Fbxl10* prevents exhaustion of the long-term repopulation potential of hematopoietic cells [48]. By contrast, gene knockdown models revealed that *Fbxl10* reduces cellular proliferation activity in MEFs and mesenchymal stem cells, accompanied by increased expression of P16 [24]. In the present study, the average expression levels of P15, P16, P19, and P21 were higher, the latter two significantly so in *Fbxl10*$^{\Delta J/\Delta J}$ GSCs than in WT GSCs (Fig. 4A). This result is consistent with our previous report that a lack of *Fbxl10-FL* causes an increase in P19 and P21 expression in MEFs [13, 27] or Embryonic Day 8.5 embryos in vivo [13]. P21 and P19, which are encoded by the *Cdkn1a* and *Cdkn2a* genes, respectively, and are markers of cellular senescence [28, 49], are negative regulators to prevent cell cycle progression from G1 to S phase. This is in agreement with the findings of the present study that in comparison to WT GSCs, the proliferation of *Fbxl10*$^{\Delta J/\Delta J}$ GSCs was significantly slower and the ratio of *Fbxl10*$^{\Delta J/\Delta J}$ GSCs in G1/G0 phase was significantly higher. On the other hand, no significant difference was observed in the ratio of apoptotic cells between *Fbxl10*$^{\Delta J/\Delta J}$ and WT GSCs, as determined by flow cytometry using an anti-cleaved CASPASE-3 antibody (Fig. 4C). This suggests that the slower proliferation of *Fbxl10*$^{\Delta J/\Delta J}$ GSCs is related to slower cell cycle progression but not to more pronounced cell death. It is notable that the correlation between *Fbxl10* and apoptosis seems to be cell type-dependent. For example, a lack of *Fbxl10* significantly increases the ratio of MEFs that undergo apoptosis [13], whereas downregulation of *Fbxl10* by gene knockdown does not significantly promote apoptosis in prostate adenocarcinoma LNCaP cells [22]. Similarly, drug-induced apoptosis is not mitigated by exogenous overexpression of *Fbxl10* in MEFs [10].

Spermatogonial cell cycle in vivo was transiently hyperactivated by treating mice with the cytotoxic agent busulfan at a modulated dose [29, 30]. By using this in vivo model, we observed that the number of undifferentiated spermatogonia did not differ between *Fbxl10*$^{\Delta J/\Delta J}$ and WT mice at 2 wk after busulfan administration, whereas there were fewer of these cells ($P = 0.08$) in *Fbxl10*$^{\Delta J/\Delta J}$ mice than in WT mice at 4 wk after treatment (Fig. 6A). Furthermore, the number of mitotically inactive undifferentiated spermatogonia, which were detected as PLZF^{+} and Ki67^{-} cells, was 10-fold higher in *Fbxl10*$^{\Delta J/\Delta J}$ mice than in WT mice, suggesting that loss of *Fbxl10-FL* dampens spermatogonial cell proliferation. Given that spermatogonial stem cells are seeds for all germ cell lineages in the testis and indispensable for sustainable spermatogenesis, the disordered proliferation of spermatogonia found in our *Fbxl10* mutant testis might be one cause of the degeneration of spermatogenesis.

We previously reported that the mRNA expression of *Fbxl10-FL* is much higher in the testis than in other organs [13]. In addition, the present data revealed that FBXL10-FL was expressed in mitotic spermatogonia and meiotic spermatocytes as well as in somatic Sertoli cells (Fig. 1B). Sertoli cells provide an essential micro-environment that supports testicular germ cell to complete the complicated process of spermatogenesis [3, 50]. Although we did not determine the function of Sertoli cells in *Fbxl10*$^{\Delta J/\Delta J}$ mice in the present study, these cells were present in seminiferous tubules that exhibited degeneration of spermatogenesis in older mice (Supplemental Fig. S2). Our in vitro study, in which the supportive effects of Sertoli cells were absent, revealed that *Fbxl10*$^{\Delta J/\Delta J}$ GSCs exhibited significantly slower proliferation and higher *P21* and *P19* expression than WT GSCs (Fig. 4, A and B). In addition, mitotically active spermatogonia was significantly fewer as well as spermatogonial cell proliferation after busulfan treatment was clearly retarded in young mice (Figs. 5 and 6) even when *Fbxl10*$^{\Delta J/\Delta J}$ mice displayed no distinct abnormality in spermatogenesis in the absence of treatment (Fig. 2C). Thus, we hypothesize that the age-dependent progression of abnormal spermatogenesis in *Fbxl10*$^{\Delta J/\Delta J}$ mice is owing, at least in part, to characteristic changes in testicular germ cells, especially in spermatogonia. Next, the contribution of Sertoli cells to spermatogenesis in this *Fbxl10*$^{\Delta J/\Delta J}$ model should be examined by transplanting *Fbxl10*$^{\Delta J/\Delta J}$ spermatogonia into WT testes or vice versa.

ACKNOWLEDGMENT

The authors thank Dr. Hirotake Ichise, Dr. Taeko Ichise, Dr. Takahiko Chimura, and Dr. Takayuki Shibasaki for their valuable advices and discussions while carrying out the research.

REFERENCES

1. Kota SK, Feil R. Epigenetic transitions in germ cell development and meiosis. Dev Cell 2010; 19:675–686.
2. Carrell DT. Epigenetics of the male gamete. Fertil Steril 2012; 97: 267–274.
3. Oatley JM, Brinster RL. The germline stem cell niche unit in mammalian testes. Physiol Rev 2012; 92:577–595.
4. Saitou M, Kagiwada S, Kurimoto K. Epigenetic reprogramming in mouse pre-implantation development and primordial germ cells. Development 2012; 139:15–31.
5. Kuroki S, Akiyoshi M, Tokura M, Miyachi H, Nakai Y, Kimura H,

Shinkai Y, Tachibana M. JMJD1C, a JmjC domain-containing protein, is required for long-term maintenance of male germ cells in mice. Biol Reprod 2013; 89:93.
6. Hayashi K, Yoshida K, Matsui Y. A histone H3 methyltransferase controls epigenetic events required for meiotic prophase. Nature 2005; 438: 374–378.
7. Glaser S, Lubitz S, Loveland KL, Ohbo K, Robb L, Schwenk F, Seibler J, Roellig D, Kranz A, Konstantinos A, Stewart AF. The histone 3 lysine 4 methyltransferase, Mll2, is only required briefly in development and spermatogenesis. Epigenet Chromatin 2009; 2:5.
8. Ciccone DN, Su H, Hevi S, Gay F, Lei H, Bajko J, Xu G, Li E, Chen T. KDM1B is a histone H3K4 demethylase required to establish maternal genomic imprints. Nature 2009; 461:415–418.
9. Frescas D, Guardavaccaro D, Bassermann F, Koyama-Nasu R, Pagano M. JHDM1B/FBXL10 is a nucleolar protein that represses transcription of ribosomal RNA genes. Nature 2007; 450:309–313.
10. Janzer A, Stamm K, Becker A, Zimmer A, Buettner R, Kirfel J. The H3K4me3 histone demethylase Fbxl10 is a regulator of chemokine expression, cellular morphology, and the metabolome of fibroblasts. J Biol Chem 2012; 287:30984–30992.
11. He J, Kallin EM, Tsukada Y, Zhang Y. The H3K36 demethylase Jhdm1b/Kdm2b regulates cell proliferation and senescence through p15(Ink4b). Nat Struct Mol Biol 2008; 15:1169–1175.
12. Liang G, He J, Zhang Y. Kdm2b promotes induced pluripotent stem cell generation by facilitating gene activation early in reprogramming. Nature Cell Biol 2012; 14:457–466.
13. Fukuda T, Tokunaga A, Sakamoto R, Yoshida N. Fbxl10/Kdm2b deficiency accelerates neural progenitor cell death and leads to exencephaly. Mol Cell Neurosci 2011; 46:614–624.
14. Kubota H, Avarbock MR, Brinster RL. Culture conditions and single growth factors affect fate determination of mouse spermatogonial stem cells. Biol Reprod 2004; 71:722–731.
15. Kubota H, Avarbock MR, Brinster RL. Growth factors essential for self-renewal and expansion of mouse spermatogonial stem cells. Proc Natl Acad Sci USA 2004; 101:16489–16494.
16. Oatley JM, Brinster RL. Spermatogonial stem cell. Methods Enzymol 2006; 419:259–282.
17. Oatley JM, Oatley MJ, Avarbock MR, Tobias JW, Brinster RL. Colony stimulating factor 1 is an extrinsic stimulator of mouse spermatogonial stem cell self-renewal. Development 2009; 136:1191–1199.
18. Araki Y, Sato T, Katagiri K, Kubota Y, Araki Y, Ogawa T. Proliferation of mouse spermatogonial stem cells in microdrop culture. Biol Reprod 2010; 83:951–957.
19. Schmittgen TD, Livak KJ. Analyzing real-time PCR data by the comparative C(T) method. Nat Protoc 2008; 3:1101–1108.
20. Kawakami E, Tokunaga A, Ozawa M, Sakamoto R, Yoshida N. The histone demethylase fbxl11/kdm2a plays an essential role in embryonic development by repressing cell-cycle regulators. Mech Develop 2014; 135:1–12.
21. Tsukada Y, Fang J, Erdjument-Bromage H, Warren ME, Borchers CH, Tempst P, Zhang Y. Histone demethylation by a family of JmjC domain-containing proteins. Nature 2006; 439:811–816.
22. Ge R, Wang Z, Zeng Q, Xu X, Olumi AF. F-box protein 10, an NF-κB-dependent anti-apoptotic protein, regulates TRAIL-induced apoptosis through modulating c-Fos/c-FLIP pathway. Cell Death Differ 2011; 18: 1–12.
23. Tzatsos A, Paskaleva P, Ferrari F, Deshpande V, Stoykova S, Contino G, Wong KK, Lan F, Trojer P, Park PJ, Bardeesy N. KDM2B promotes pancreatic cancer via Polycomb-dependent and -independent transcriptional programs. J Clin Invest 2013; 123:727–739.
24. Tzatsos A, Paskaleva P, Lymperi S, Contino G, Stoykova S, Chen Z, Wong KK, Bardeesy NA. Lysine (K)-specific demethylase 2B (KDM2B)-let-7-Enhancer of Zester Homolog 2 (EZH2) pathway regulates cell cycle progression and senescence in primary cells. J Biol Chem 2011; 286: 33061–33069.
25. Kanatsu-Shinohara M, Ogunuki N, Inoue K, Miki H, Ogura A, Tokyokuni S, Shinohara T. Long-term proliferation in culture and germline transmission of mouse male germline stem cells. Biol Reprod 2003; 69: 612–616.
26. Molofsky AV, He S, Bydon M, Morrison SJ, Pardal R. Bmi-1 promotes neural stem cell self-renewal and neural development but not mouse growth and survival by repressing the p16Ink4a and p19Arf senescence pathways. Genes Dev 2005; 19:1432–1437.
27. Tzatsos A, Pfau R, Kampranis SC, Tsichlis PN. Ndy1/KDM2B immortalizes mouse embryonic fibroblasts by repressing the *Ink4a*/*Arf* locus. Proc Natl Acad Sci U S A 2009; 106:2641–2646.
28. Salama R, Sadaie M, Hoare M, Narita M. Cellular senescence and its effector programs. Genes Dev 2014; 28:99–114.
29. Masuda T, Itoh K, Higashitsuji H, Higashitsuji H, Nakazawa N, Sakurai T, Liu Y, Tokuchi H, Fujita T, Zhao Y, Nishiyama H, Tanaka T, et al. Cold-inducible RNA-binding protein (Cirp) interacts with Dyrk1b/Mirk and promotes proliferation of immature male germ cells in mice. Proc Natl Acad Sci U S A 2012; 109:10885–10890.
30. Chakraborty P, Buaas FW, Sharma M, Snyder E, de Rooij DG, Braun RE. LIN28A marks the spermatogonial progenitor population and regulates its cyclic expansion. Stem Cells 2014; 32:860–873.
31. Takubo K, Ohmura M, Azuma M, Nagamatsu G, Yamada W, Arai F, Hirao A, Suda T. Stem cell defects in ATM-deficient undifferentiated spermatogonia through DNA damage-induced cell-cycle arrest. Cell Stem Cell 2008; 2:170–182.
32. Blackledge NP, Farcas AM, Kondo T, King HW, McGouran JF, Hanssen LLP, Ito S, Cooper S, Kondo K, Keseki Y, Ishikura T, Long HK, et al. Variant PRC1 complex-dependent H2A ubiquitylation drives PRC2 recruitment and Polycomb domain formation. Cell 2014; 157:1–15.
33. Boulard M, Edwards JR, Bestor TH. FBXL10 protects Polycomb-bound genes from hypermethylation. Nat Genet 2015; 47:479–485.
34. Cole F, Baudat F, Grey C, Keeney S, de Massy B, Jasin M. Mouse tetrad analysis provides insights into recombination mechanisms and hotspot evolutionary dynamics. Nat Genet 2014; 46:1072–1080.
35. Baker CL, Kajita S, Walker M, Saxl RL, Raghupathy N, Choi K, Petkov PM, Paigen K. PRDM9 drives evolutionary erosion of hotspots in *Mus musculus* through haplotype-specific initiation of meiotic recombination. PLoS Genet 2015; 11:e1004916.
36. Jenuwein T, Allis CD. Translating the histone code. Science 2001; 293: 1074–1080.
37. Sims RJ III, Nishioka K, Reinberg D. Histone lysine methylation: a signature for chromatin function. Trends Genet 2003; 19:629–639.
38. Iwamori N, Zhao M, Meistrich ML, Matzuk MM. The testis-enriched histone demethylase, KDM4D, regulates methylation of histone H3 lysine 9 during spermatogenesis in the mouse but is dispensable for fertility. Biol Reprod 2011; 84:1225–1234.
39. Buaas FW, Kirsh AL, Sharma M, McLean DJ, Morris JL, Griswold MD, de Rooij DG, Braun RE. Plzf is required in adult male germ cells for stem cell self-renewal. Nat Genet 2004; 36:647–652.
40. Costoya JA, Hobbs RM, Barna M, Cattoretti G, Manova K, Sukhwani M, Orwig KE, Wolgemuth DJ, Pandolfi PP. Essential role of Plzf in maintenance of spermatogonial stem cells. Nat Genet 2004; 36:653–659.
41. Hobbs RM, Seandel M, Falciatori I, Rafii S, Pandolfi PP. Plzf regulates germline progenitor self-renewal by opposing mTORC1. Cell 2010; 142: 468–479.
42. Jain S, Naughton CK, Yang M, Strickland A, Vij K, Encinas M, Milbrandt J. Mice expressing a dominant-negative Ret mutation phenocopy human Hirschsprung disease and delineate a direct role of Ret in spermatogenesis. Development 2004; 131:5503–5513.
43. Jijiwa M, Kawai K, Fukihara J, Nakamura A, Hasegawa M, Suzuki C, Takahashi M. GDNF-mediated signaling via RET tyrosine 1062 is essential for maintenance of spermatogonial stem cells. Genes Cells 2008; 13:365–374.
44. Morales C, Griswold MD. Retinol-induced stage synchronization in seminiferous tubules of the rat. Endocrinology 1987; 121:432–434.
45. van Pelt AM, de Rooij DG. Synchronization of the seminiferous epithelium after vitamin A replacement in vitamin A-deficient mice. Biol Reprod 1990; 43:363–367.
46. Yang QE, Racicot KE, Kaucher AV, Oatley MJ, Oatley JM. MicroRNAs 221 and 222 regulate the undifferentiated state in mammalian male germ cells. Development 2013; 140:280–290.
47. Schmidt JA, Abramowitz LK, Kubota H, Wu X, Niu Z, Avarbock MR, Tobias JW, Bartolomei MS, Brinster RL. In vivo and in vitro aging is detrimental to mouse spermatogonial stem cell function. Biol Reprod 2011; 84:698–706.
48. Konuma T, Nakamura S, Miyagi S, Negishi M, Chiba T, Oguro H, Yuan J, Mochizuki-Kashio M, Ichikawa H, Miyoshi H, Vidal M, Iwama A. Forced expression of the histone demethylase Fbxl10 maintains self-renewing hematopoietic stem cells. Exp Hematol 2011; 39:697–709.
49. Ishimura, A, Minehata, K, Terashima, M, Kondoh G, Hara T, Suzuki T. Jmjd5, an H3K36me2 histone demethylase, modulates embryonic cell proliferation through the regulation of Cdkn1a expression. Development 2012; 139:749–759.
50. Kanatsu-Shinohara M, Shinohara T. Spermatogonial stem cell self-renewal and development. Annu Rev Cell Dev Biol 2013; 29:163–187.